Faddeev approach to the reaction $K^-d \to \pi\Sigma n$ at $p_K = 1\,\mathrm{GeV}/c$

K. Miyagawa,[1] J. Haidenbauer,[2] and H. Kamada[3]

[1]*Graduate School of Science, Okayama University of Science, 1-1 Ridai-cho, Okayama 700-0005, Japan*

[2]*Institute for Advanced Simulation, Institut für Kernphysik, and Jülich Center for Hadron Physics, Forschungszentrum Jülich, D-52425 Jülich, Germany*

[3]*Department of Physics, Faculty of Engineering, Kyushu Institute of Technology, KitaKyushu 804-8550, Japan*

(Received 2 March 2018; published 11 May 2018)

The reaction $K^-d \to \pi\Sigma n$ is studied within a Faddeev-type approach, with emphasis on the specific kinematics of the E31 experiment at J-PARC, i.e., K^- beam momentum of $p_K = 1$ GeV/c and neutron angle of $\theta_n = 0^\circ$. The employed Faddeev approach requires as main input amplitudes for the two-body subsystems $\bar{K}N \to \bar{K}N$ and $\bar{K}N \to \pi\Sigma$. For the latter, results from recently published chiral unitary models of the $\bar{K}N$ interaction are utilized. The $\bar{K}N \to \bar{K}N$ amplitude itself, however, is taken from a recent partial-wave analysis. Because of the large incoming momentum of the K^-, the $\bar{K}N$ interaction is probed in a kinematical regime where those chiral potentials are no longer applicable. A comparison of the predicted spectrum for various $\pi\Sigma$ charge channels with preliminary data is made and reveals a remarkable agreement as far as the magnitude and the line shape in general is concerned. Noticeable differences observed in the $\pi\Sigma$ spectrum around the $\bar{K}N$ threshold, i.e. in the region of the $\Lambda(1405)$ resonance, indicate a sensitivity to the details of the employed $\bar{K}N \to \pi\Sigma$ amplitudes and suggest that pertinent high-precision data could indeed provide substantial constraints on the structure of the $\Lambda(1405)$.

DOI: 10.1103/PhysRevC.97.055209

I. INTRODUCTION

Modern and systematic approaches that exploit the (approximate) chiral and SU(3) flavor symmetries of the underlying QCD Lagrangian have significantly improved our understanding of the $\bar{K}N$ interaction for energies in the vicinity of its threshold; see Refs. [1–3] for recent overviews. Nonetheless, some essential questions remain. One of them is the detailed pole structure of the $\Lambda(1405)$, a resonance which is located below but not far from the $\bar{K}N$ threshold. Another closely connected topic is the possible existence of (so-called) quasibound states of the K^-NN system [4,5] and/or of kaons with heavier nuclei. A summary of predictions and references to the various works can be found in Refs. [6,7].

Though chiral SU(3) dynamics provides strong constraints on the $\bar{K}N$ interaction, there are still fairly large differences in the actual results and predictions, as one can easily see from scanning through the pertinent literature. This reflects the complexity of the underlying physics and is due to the fact that $\bar{K}N$ cannot be considered as an isolated system. Possible couplings to the $\pi\Lambda$ and $\pi\Sigma$ systems, whose thresholds are just about 100–200 MeV lower, strongly influence the dynamics. Most of the available experimental information comes from studies of K^-p induced reactions (K^-p elastic scattering, $K^-p \to \bar{K}^0n$, $K^-p \to \pi^0\Lambda$, and $K^-p \to \pi\Sigma$). Thus, only isospin combinations of the amplitudes are constrained by data but not the individual amplitudes themselves. As a consequence, there are large variations between the isospin $I = 1$ $\bar{K}N$ (K^-n) amplitudes around and below the threshold, as exemplified, e.g., in Fig. 2 of Ref. [2], despite that all considered interactions are constrained from chiral SU(3) dynamics. Actually even for K^-p there is agreement only for energies at and above the threshold (cf. the same figure), owing to experimental information on the level shift and width of kaonic hydrogen [8], and the aforementioned data for K^-p elastic scattering. The differences in the energy dependence below the threshold reflect variations in the position of the two poles that are a characteristic feature of the $\Lambda(1405)$ within chiral approaches [9–14] (but appear also in conventional meson-exchange dynamics [15–17]). Here specifically the pole with the lower mass is prone to the very details of how chiral SU(3) dynamics is implemented and has been predicted to be basically anywhere between the $\pi\Sigma$ and $\bar{K}N$ thresholds [1–3].

Currently there are major experimental efforts to provide further constraints on the $\bar{K}N$ interaction. One of them concerns plans for measuring the level shift of K^-d atoms in order to pin down the $I = 1$ $\bar{K}N$ amplitude [18]. Access to the energy dependence of the amplitudes below the $\bar{K}N$ threshold and thus to quantitative information on the pole structure of the $\Lambda(1405)$ is possible in studies of the $\pi\Sigma$ system. Several experiments with that aim have been already performed over the past few years. Specifically, this concerns measurements of the $\pi\Sigma$ invariant mass spectrum in photon-induced [19,20] and electron-induced [21] production on the proton, in the reaction $pp \to pK^+\pi\Sigma$ [22,23], and finally in K^- induced reactions on a proton [24] or deuteron target [25,26].

In the present work, we focus on the reaction $K^-d \to \pi\Sigma n$ which is the objective of the E31 experiment at J-PARC [27]. The experiment is performed for specific kinematics, namely for a K^- beam momentum of $p_K = 1$ GeV/c and a neutron angle of $\theta_n = 0^\circ$. Preliminary data for the reaction channels $K^-d \to \pi^\pm\Sigma^\mp n$, $K^-d \to \pi^0\Sigma^0 n$, and $K^-d \to \pi^-\Sigma^0 p$ have been already presented at conferences [26] and in proceedings [25] and final results are to be expected

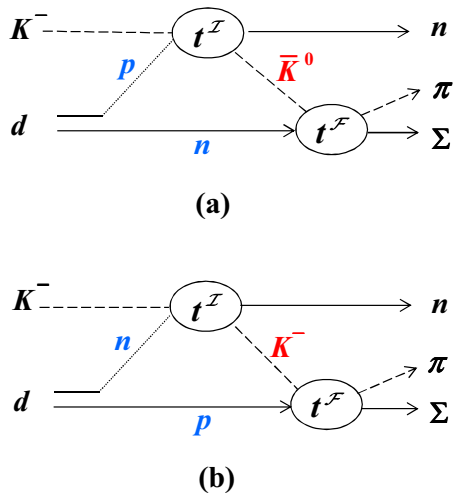

FIG. 1. Mechanisms considered in the calculation of the reaction $K^-d \to \pi\Sigma n$: (a) $\bar{K}^0 n \to \pi\Sigma$ rescattering and (b) $K^-p \to \pi\Sigma$ rescattering.

soon. Thus, there is a strong motivation to catch up with this development and to perform calculations that are sophisticated enough to facilitate a sensible confrontation of theoretical predictions with empirical information. In the context of the E31 experiment, this implies that the three-body character of the reaction has to be accounted for and the formalism best suited for that is the one proposed by Faddeev. Indeed, in the past some calculations for $K^-d \to \pi\Sigma n$ have been presented based on a Faddeev-type approach [28–30], whereas others [31–34], including our own initial study [31], took into account only the first terms in the multiscattering expansion, which are depicted in Fig. 1.

Among the studies of the reaction $K^-d \to \pi\Sigma n$, the most instructive one so far is certainly the work of Kamano and Lee [34]. Their calculation, based on the diagrams depicted in Fig. 1, revealed that the $\bar{K}N \to \bar{K}N$ amplitude that appears in the first step of the two-step process ($t^{\mathcal{I}}$ in Fig. 1) plays an essential role. In particular, this study demonstrated that higher partial waves have to be included in this amplitude in the calculation of $K^-d \to \pi\Sigma n$. Only then reaction cross section with a magnitude comparable to the experiment are obtained. Truncating the $\bar{K}N$ amplitude to the s waves, so far done in $K^-d \to \pi\Sigma n$ calculations based on chiral potentials, not least because in general those models generate s waves only, leads to a gross underestimation of the empirical information [30].

In the present K^-d calculation, we take this important aspect into account and include higher partial waves in the $\bar{K}N \to \bar{K}N$ amplitude. Furthermore, we go beyond the two-step approximation of our earlier study [31] and treat the $\bar{K}NN$ three-body scattering process rigorously. Since we want to investigate to what extent the $\pi\Sigma$ invariant mass spectrum around the $\bar{K}N$ threshold is sensitive to the details of the $\bar{K}N$ interaction, i.e., to the structure of the $\Lambda(1405)$, we employ different chiral potentials taken from the literature, notably the ones of Cieplý and Smejkal [35] and Ohnishi *et al.* [30]. Both incorporate the so-called Weinberg-Tomozawa term, i.e., the leading-order piece of the effective chiral meson-baryon Lagrangian. Furthermore, we consider the chiral interaction proposed by Oset *et al.* [10] which we had used in our initial studies of the reaction $K^-d \to \pi\Sigma n$ [29,31].

The paper is structured in the following way: Our calculations are performed within a Faddeev-type approach and the details of the employed formalism are outlined in Sec. II. Further details can be found in two appendixes. In Sec. III, we summarize information about the employed input for the two-body amplitudes $\bar{K}N \to \bar{K}N$ and $\bar{K}N \to \pi\Sigma$. Some characteristic results of these two-body amplitudes are likewise provided. Our results for the reaction $K^-d \to \pi\Sigma n$ are given and discussed in Sec. IV. The paper ends with a summary.

II. FORMULATION OF THE $K^-d \to \pi\Sigma n$ REACTION

A. Faddeev equations

We derive the $K^-d \to \pi\Sigma n$ amplitude based on the Faddeev equations for the $\bar{K}NN - \pi\Sigma N$ coupled system. The nucleon which appears in the $\pi\Sigma N$ system can be either of the two present in the $\bar{K}NN$ system. Clearly, the $\bar{K}NN$ part of the wave function has to be antisymmetrical under exchange of the two nucleons, and hence the part describing $\pi\Sigma N$ must reflect it. This feature can be formulated explicitly by the generalized Pauli principle introduced in Ref. [36].

Let us first write down the Faddeev equations for a meson numbered 1 and two baryons numbered 2 and 3:

$$|\psi^{(23)}\rangle = |\phi\rangle + G_0\, t_{23}\ \ (|\psi^{(12)}\rangle + |\psi^{(13)}\rangle), \tag{1}$$

$$|\psi^{(12)}\rangle = G_0\, t_{12}\ \ (|\psi^{(23)}\rangle + |\psi^{(13)}\rangle), \tag{2}$$

$$|\psi^{(13)}\rangle = G_0\, t_{13}\ \ (|\psi^{(23)}\rangle + |\psi^{(12)}\rangle), \tag{3}$$

where ϕ indicates an incoming wave, and t_{ij} are the two-body transition operators embedded in the three-particle space. The total wave function ψ is the sum of the three components:

$$|\psi\rangle = |\psi^{(23)}\rangle + |\psi^{(12)}\rangle + |\psi^{(13)}\rangle\,.$$

For the $\bar{K}NN - \pi\Sigma N$ system, we introduce particle labels, in addition to the usual space and spin labels, in the form of $|\,a\alpha\beta\rangle$ [36]. The particle labels denote $\{a\alpha\beta\} = \{KNN, \pi\Sigma N, \pi N\Sigma\}$, and the state $|\,a\alpha\beta\rangle$ stands for $|a\rangle_1\,|\alpha\rangle_2\,|\beta\rangle_3$. The completeness relation in that particle space is given by

$$|\bar{K}NN\rangle\,\langle\bar{K}NN| + |\pi\Sigma N\rangle\,\langle\pi\Sigma N| + |\pi N\Sigma\rangle\,\langle\pi N\Sigma| = 1.$$

Using the basis above, one can construct a fully symmetric Hamiltonian with regard to two baryons and a corresponding antisymmetric wave function (for more details, see Ref. [36]).

Let us impose antisymmetry, $P_{23}\,|\psi\rangle = -\,|\psi\rangle$, where the operator P_{23} indicates the permutation of particles 2 and 3. Then we have the antisymmetric relations between the Faddeev components:

$$P_{23}\,|\psi^{(23)}\rangle = -\,|\psi^{(23)}\rangle\,, \quad P_{23}\,|\psi^{(12)}\rangle = -\,|\psi^{(13)}\rangle\,.$$

Taking particle representations for the Faddeev equations (1)–(3) with the above antisymmteric relations, one can derive the following coupled equations for the five independent

components:

$$\psi^{(23)}_{\bar{K}NN} = \phi_{K^-d} + G_0(\bar{K}NN)\, t_{NN}(23)(1 - P_{23})\, \psi^{(12)}_{\bar{K}NN}, \quad (4)$$

$$\psi^{(12)}_{\bar{K}NN} = G_0(\bar{K}NN)\, t_{\bar{K}N,\bar{K}N}(12)\big(\psi^{(23)}_{\bar{K}NN} - P_{23}\, \psi^{(12)}_{\bar{K}NN}\big) + G_0(\bar{K}NN)\, t_{\bar{K}N,\pi\Sigma}(12)\big(\psi^{(23)}_{\pi\Sigma N} + \psi^{(13)}_{\pi\Sigma N}\big), \quad (5)$$

$$\psi^{(12)}_{\pi\Sigma N} = G_0(\pi\Sigma N)\, t_{\pi\Sigma,\bar{K}N}(12)\big(\psi^{(23)}_{\bar{K}NN} - P_{23}\, \psi^{(12)}_{\bar{K}NN}\big) + G_0(\pi\Sigma N)\, t_{\pi\Sigma,\pi\Sigma}(12)\big(\psi^{(23)}_{\pi\Sigma N} + \psi^{(13)}_{\pi\Sigma N}\big), \quad (6)$$

$$\psi^{(23)}_{\pi\Sigma N} = G_0(\pi\Sigma N)\; t_{\Sigma N}(23)\big(\psi^{(12)}_{\pi\Sigma N} + \psi^{(13)}_{\pi\Sigma N}\big), \quad (7)$$

$$\psi^{(13)}_{\pi\Sigma N} = G_0(\pi\Sigma N)\; t_{\pi N}(13)\big(\psi^{(12)}_{\pi\Sigma N} + \psi^{(23)}_{\pi\Sigma N}\big), \quad (8)$$

where the components are defined as, for example, $\psi^{(23)}_{\bar{K}NN} = \langle \bar{K}NN|\, \psi^{(23)}\rangle$.

It is a standard procedure [36,37] to extract various partial breakup amplitudes from each individual kernel part of the set (4)–(8). Those are introduced into Eqs. (1)–(3) as

$$|\psi^{(23)}\rangle = |\phi\rangle + G_0\, T^{(23)}\, |\phi\rangle\,, \quad (9)$$

$$|\psi^{(ij)}\rangle = G_0\, T^{(ij)}\, |\phi\rangle\,, \quad (ij) = (12),(13)\,. \quad (10)$$

Projecting these equations onto particle states, one can derive the following coupled equations for partial breakup amplitudes which have the same structure as the set (4)–(8):

$$T^{(23)}_{\bar{K}NN} = t_{NN}(23)\, G_0(\bar{K}NN)\;\; (1 - P_{23})\, T^{(12)}_{\bar{K}NN}, \quad (11)$$

$$T^{(12)}_{\bar{K}NN} = t_{\bar{K}N,\bar{K}N}(12)\, \phi_d + t_{\bar{K}N,\bar{K}N}(12)\, G_0(\bar{K}NN)\big(T^{(23)}_{\bar{K}NN} - P_{23}\, T^{(12)}_{\bar{K}NN}\big) + t_{\bar{K}N,\pi\Sigma}(12)\, G_0(\pi\Sigma N)\big(T^{(23)}_{\pi\Sigma N} + T^{(13)}_{\pi\Sigma N}\big), \quad (12)$$

$$T^{(12)}_{\pi\Sigma N} = t_{\pi\Sigma,\bar{K}N}(12)\, \phi_d + t_{\pi\Sigma,\bar{K}N}(12)\, G_0(\bar{K}NN)\big(T^{(23)}_{\bar{K}NN} - P_{23}\, T^{(12)}_{\bar{K}NN}\big) + t_{\pi\Sigma,\pi\Sigma}(12)\, G_0(\pi\Sigma N)\big(T^{(23)}_{\pi\Sigma N} + T^{(13)}_{\pi\Sigma N}\big), \quad (13)$$

$$T^{(23)}_{\pi\Sigma N} = t_{\Sigma N}(23)\, G_0(\pi\Sigma N)\big(T^{(12)}_{\pi\Sigma N} + T^{(13)}_{\pi\Sigma N}\big), \quad (14)$$

$$T^{(13)}_{\pi\Sigma N} = t_{\pi N}(13)\, G_0(\pi\Sigma N)\big(T^{(12)}_{\pi\Sigma N} + T^{(23)}_{\pi\Sigma N}\big), \quad (15)$$

where the partial amplitudes are defined as, for example, $T^{(23)}_{\bar{K}NN} = \langle \bar{K}NN|\, T^{(23)}|\phi\rangle$, and ϕ_d is the deuteron wave function. The breakup amplitude into the "physical" $\pi\Sigma N$ channel is obtained by

$$\begin{aligned} T(K^- d \to \pi\Sigma N) &= \langle \pi\Sigma N|\frac{1 - P_{23}}{\sqrt{2}}(T^{(12)} + T^{(23)} + T^{(13)})|\,\phi\rangle \\ &= \sqrt{2}\big\{T^{(12)}_{\pi\Sigma N} + T^{(23)}_{\pi\Sigma N} + T^{(13)}_{\pi\Sigma N}\big\}. \end{aligned} \quad (16)$$

B. Technicalities and relativity

Here we explain some details concerning the numerical treatment and relativity in solving the Faddeev-type equations (11)–(15). Let us illustrate them, taking one of the kernel parts of Eq. (12), for example,

$$T^{(12)}_{\bar{K}NN} = t_{\bar{K}N,\bar{K}N}(12)\, G_0(\bar{K}NN)\big(-P_{23}\, T^{(12)}_{\bar{K}NN}\big). \quad (17)$$

We work in the three-body center-of-mass (c.m.) system throughout this paper, denote the momentum of particle i by $\vec{q}_i$ $(i = 1,2,3)$, and use the partial-wave projected momentum space basis

$$|k\, q\;\alpha\rangle \equiv |k\, q\,;\, (ls)j\;(\lambda\, s_3)j_s\;J\rangle, \quad (18)$$

where α indicates various angular momenta in a jJ coupling: two-body quantum numbers $(ls)j$, quantum numbers referred to the third particle $(\lambda\, s_3)j_s$, and total angular momentum J. In the nonrelativistic case, k and q correspond to the magnitudes of standard Jacobi momenta, but now in a relativistic generalization, $\vec{k}$ and $-\vec{k}$ are momenta of particle 1 and 2 in the c.m. frame of the two-particle subsystem, and $\vec{q}$ indicates the third particle momentum $\vec{q}_3$. The momentum $\vec{k}$ is related to the three-body c.m. momenta $\vec{q}_1$ and $\vec{q}_2$ in a compact expression [38] by

$$\vec{k} = \frac{\varepsilon_2\, \vec{q}_1 - \varepsilon_1\, \vec{q}_2}{\varepsilon_1 + \varepsilon_2}\,, \quad (19)$$

where $\varepsilon_i = (\omega_i + u_i)/2$, $\omega_i \equiv \sqrt{q_i^2 + m_i^2}$, and $u_i \equiv \sqrt{k^2 + m_i^2}$.

Projecting Eq. (17) onto the basis above, we obtain

$$\begin{aligned} &\big\langle k\, q\, \alpha \,\big|\, T^{(12)}_{\bar{K}NN}\big\rangle \\ &= \sum_{\alpha'} \int k'^2 dk'\, \langle k\,\alpha|\, t_{12}(q)|\, k'\alpha'\rangle \\ &\quad \times \frac{1}{W - \omega_3(q) - \omega_{12}(q,k') + i\epsilon} \\ &\quad \times \sum_{\alpha''} \int k''^2 dk'' \int q''^2 dq''\, \langle k' q\, \alpha'|\, P_{23}|\, k'' q'' \alpha''\rangle \\ &\quad \times \big(-\big\langle k'' q'' \alpha'' \,\big|\, T^{(12)}_{\bar{K}NN}\big\rangle\big), \end{aligned} \quad (20)$$

where W denotes the total energy, and $\omega_3(q) = \sqrt{q^2 + m_3^2}$, $\omega_{12}(q,k') \equiv \sqrt{q^2 + W_{12}^2}$, and $W_{12} \equiv \sqrt{k'^2 + m_1^2} + \sqrt{k'^2 + m_2^2}$. The permutation matrix element $\langle k' q\, \alpha'|\, P_{23}|\, k'' q'' \alpha''\rangle$ on the right-hand side describes a rearrangement between different types of basis states $|\, k' q\, \alpha'\rangle$ and $P_{23}\,|\, k'' q'' \alpha''\rangle$, which is evaluated as

$$\begin{aligned} &\langle k' q\, \alpha'\,|\, P_{23}|\, k'' q'' \alpha''\rangle \\ &= \int_{-1}^{1} dx\, \frac{\delta(q'' - \chi)}{q''^2}\, \frac{\delta(k'' - \pi)}{k''^2}\, R_{\alpha'\alpha''}(k' q\, x)\,, \end{aligned} \quad (21)$$

where χ and π are shifted momenta given by

$$\chi = \sqrt{k'^2 + (\rho\, q)^2 - 2k'\rho q\, x}, \quad (22)$$

$$\pi = \sqrt{(\rho'' k')^2 + (1 - \rho''\rho)^2 q^2 - 2\rho'' k'(1 - \rho''\rho) q\, x}. \quad (23)$$

The derivation of Eq. (21) including the expressions of $R_{\alpha'\alpha''}(k' q\, x)$, ρ, and ρ'' are given in Appendix A. Note that in the relativistic case, ρ and ρ'' are no longer constants but depend on k', q, and x.

In Eq. (20), together with Eq. (21), four integrations over k', k'', q'', and x are left, but we perform the k'' and x integrations analytically using the two δ functions, which enables us [39]

to avoid the complicated singularity pattern (with moving logarithmic singularities) in standard approaches. The resulting form is

$$\begin{aligned}\left\langle k\,q\,\alpha\,\middle|\,T^{(12)}_{\bar{K}NN}\right\rangle = &\sum_{\alpha'}\int_0^\infty k'dk'\,\langle k\,\alpha|\,t_{12}(q)|\,k'\alpha'\rangle\\ &\times\frac{1}{W-\omega_3(q)-\omega_{12}(q,k')+i\epsilon}\\ &\times\sum_{\alpha''}\int_{|k'-\rho_+\,q|}^{k'+\rho_-\,q}q''dq''\frac{1}{\rho\,q\,f_r}R_{\alpha'\alpha''}(k'q\,x_0)\\ &\times\left(-\left\langle\pi\,\chi\,\alpha''\,\middle|\,T^{(12)}_{\bar{K}NN}\right\rangle\right),\end{aligned}\tag{24}$$

where x_0 and the factor f_r, which is special in the relativistic case, are functions of k', q, and q'', while ρ_- and ρ_+ are functions of k' and q. Those expressions are given in Appendix B. Note that only a simple pole in the k' variable appears positioned at k_0 which satisfies the relation

$$\sqrt{(W-\omega_3(q))^2-q^2}=\sqrt{k_0^2+m_1^2}+\sqrt{k_0^2+m_2^2}\,,$$

giving the zero of the energy denominator. This new prescription of keeping the k' and q'' integrations, which was introduced in Sec. 2.2 of Ref. [39] and is extended here to the relativistic case, greatly reduces the numerical complications.

Finally, we mention that the boosted two-body t-matrix $\langle k\,\alpha|\,t_{12}(q)|\,k'\alpha\rangle$ describes transitions in the moving frame with the magnitude of the momentum given by the modulus $|\vec{q}_1+\vec{q}_2|=|-\vec{q}\,|$. Following the procedure of a Poincaré invariant few-body model developed in Ref. [40], it is related to the t matrix $\langle k\,\alpha|\,t^{\rm cm}_{12}|\,k'\alpha\rangle$ defined in the c.m. frame of the two particles 1 and 2 as

$$\langle k\,\alpha|\,t_{12}(q)|\,k'\alpha\rangle=\frac{W_{12}(k)+W_{12}(k')}{\omega_{12}(q,k)+\omega_{12}(q,k')}\,\langle k\,\alpha|\,t^{\rm cm}_{12}|\,k'\alpha\rangle\,,\tag{25}$$

where $W_{12}(k)\equiv\sqrt{k^2+m_1^2}+\sqrt{k^2+m_2^2}$, and the two-body energy for $\langle k\,\alpha|\,t^{\rm cm}_{12}|\,k'\alpha\rangle$ is determined as $\sqrt{[W-\omega_3(q)]^2-q^2}$. The expression (25) only holds for half-off-shell t matrices (see Eq. (48) of Ref. [40]) but at this stage we use it also for fully off-shell t matrices as an approximation. The prescription for fully off-shell t matrices has been studied in Refs. [40] and [41].

III. EMPLOYED TWO-BODY AMPLITUDES

There is an abundance of studies of the $\bar{K}N$ interaction that start out from an effective chiral Lagrangian—either at leading order or up to next-to-leading order, and considering the coupling to the $\pi\Lambda$ and $\pi\Sigma$ channels or even to all meson-baryon systems with strangeness $S=-1$ that can be build from the lowest SU(3) (pseudoscalar meson, baryon) octets [1–3,9–14]. However, only some of the resulting interactions can be readily adapted to match with the Faddeev-type three-body approach described above. Calculations in that scheme require as input two-body amplitudes that are generated from a potential inserted into a standard (relativistc or nonrelativistic) three-dimensional Lippmann-Schwinger equation so that the pertinent reaction amplitudes can be calculated for momenta that are on- or off the energy shell. It is worth mentioning that the very first study of the $\bar{K}N$ interaction based on a chiral Lagrangian [42] yielded indeed such a potential.

TABLE I. Characteristic results for the considered $\bar{K}N$ potentials by Cieplý and Smejkal (TW1) [35], Ohnishi *et al.* ($V^{E\text{-dep.}}$) [30], and Oset-Ramos-Bennhold (ORB) [10]. Scattering lengths are in fm and pole positions are in MeV.

Model	$a_{\bar{K}N}$ $(I=0)$	$a_{\bar{K}N}$ $(I=1)$	Pole 1	Pole 2
TW1	$-1.61+i\,1.02$	$0.60+i\,0.50$	$1433-i\,25$	$1371-i\,54$
$V^{E-\text{dep.}}$	$-1.89+i\,1.11$	$0.45+i\,0.53$	$1429-i\,15$	$1344-i\,49$
ORB	$-1.72+i\,0.89$	$0.52+i\,0.64$	$1426-i\,16$	$1390-i\,66$

In the present study, we utilize two fairly recent potentials, namely the model TW1 (also known as $\rm P_{WT}$) by Cieplý and Smejkal [35], and the energy-dependent model $V^{E-\text{dep.}}$ of Ohnishi *et al.* [30]. Both are so-called chirally motivated potentials, i.e., they are based on the Weinberg-Tomozawa term, and both yield results in agreement with the latest experimental value for the level shift and width of kaonic hydrogen by the Siddharta Collaboration [8]. The latter aspect is very important because those data put very tight constraints on the K^-p scattering length, i.e., on the $\bar{K}N$ interaction close to the threshold. The actual expressions for those potentials can be found in Refs. [35] and [30], respectively, together with pertinent results for $\bar{K}N$ and $\bar{K}N\to\pi\Sigma$ (see also Refs. [43] and [14]). The formal difference between the two potentials is very small, consisting only in the treatment of the factors coming from the energies of the mesons and baryons, cf. Eqs. (1) [35] and (17) [30], respectively. However, the actual fits to the data are different and so are the underlying two-body amplitudes. As examples, we show the ones for $\bar{K}N\to\pi\Sigma$ in Fig. 2. Some key results like the $\bar{K}N$ scattering lengths and the pole positions of the $\Lambda(1405)$ are summarized in Table I. Besides those interactions we consider also the Oset-Ramos-Bennhold (ORB) potential [10]. This is done mainly for historical reasons. We used this potential in our initial study of $K^-d\to\pi\Sigma n$ [31] and we wanted to connect with those results. Note that the K^-p scattering length predicted by the ORB potential is not in line with the kaonic hydrogen results [8]. Still, it will be interesting to see in how far the $K^-d\to\pi\Sigma n$ results differ from those for the other potentials.

As already mentioned, typically chiral potentials are limited to s waves only. Accordingly, in view of the findings of Kamano and Lee [34], these are not suitable for generating the $\bar{K}N$ amplitude that enters into the initial scattering process ($t^{\mathcal{I}}$ in Fig. 1). Thus, in order to circumvent this difficulty, we decided to resort to a phenomenological treatment which means that we substitute this amplitude directly by results of a partial-wave analysis of available $\bar{K}N$ scattering data, namely the one performed recently by Manley and his group at Kent State University (KSU) [44]. This analysis covers the energy range from 1480 to 2100 MeV, i.e., goes well beyond $p_{K^-}=1$ GeV/c (corresponding to a $\bar{K}N$ c.m. energy of 1795 MeV) that is needed for analyzing the E31 experiment. Using those results has the advantages that one implements an amplitude that yields an excellent reproduction of the $\bar{K}N$ data and that one

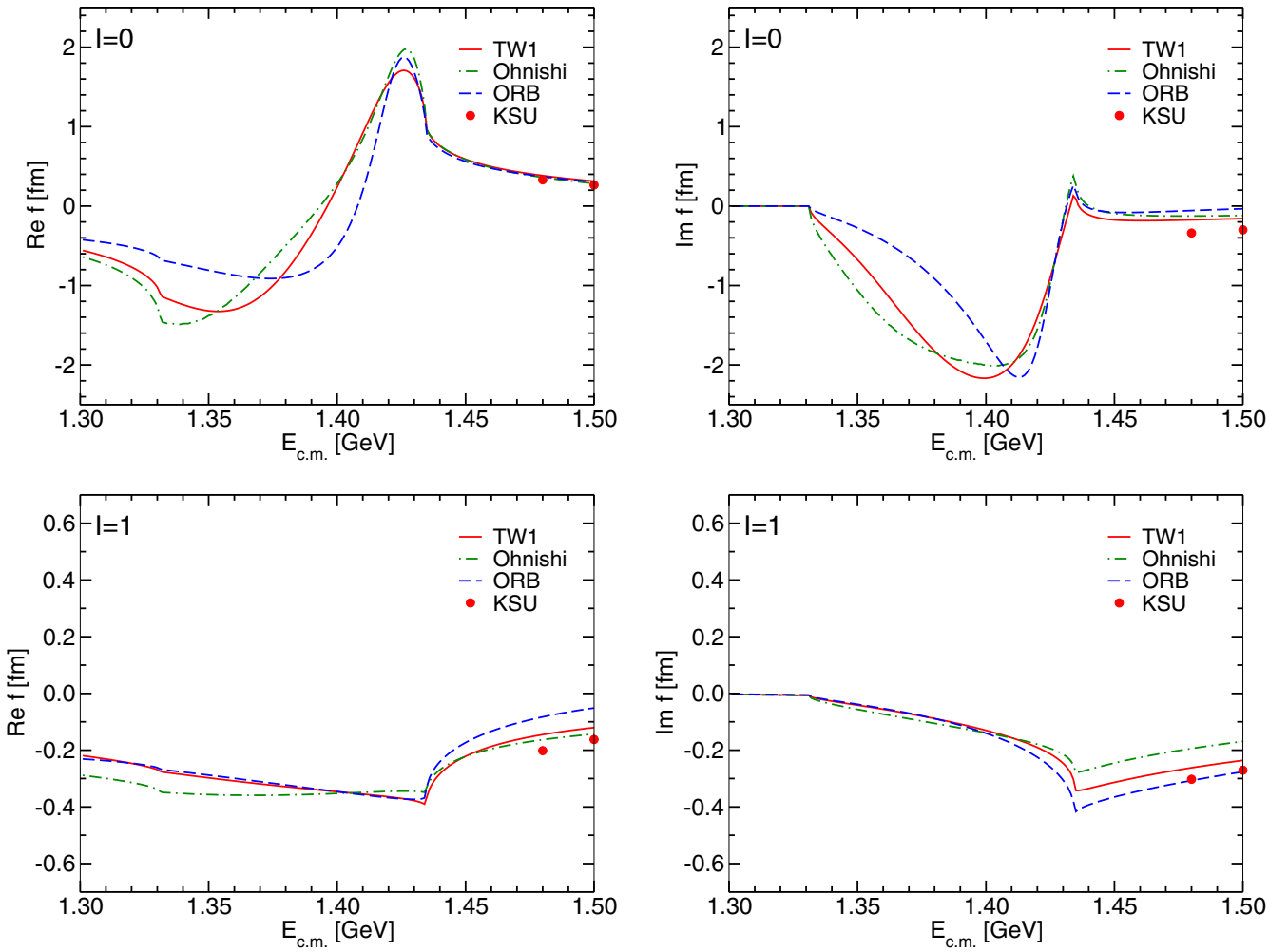

FIG. 2. $\bar{K}N \to \pi\Sigma$ isospin $I = 0,1$ s-wave amplitudes of the employed potentials: TW1 [35] (solid lines), Ohnishi *et al.* [30] (dash-dotted lines), and ORB [10] (dashed lines) and of the KSU analysis [44] (filled circles).

can use as many partial waves as are needed in the three-body calculation for getting converged results for the considered observables. Of course, there is a price we have to pay. We have to introduce a phenomenological form factor for the required off-shell extension. To be concrete, we use the form factor $f(p,k) = \Lambda^2/[\Lambda^2 + (p-k)^2]$, which depends on the off-shell momentum p but also on the on-shell momentum k. This choice ensures that the $\bar{K}N$ on-shell amplitude remains unchanged. For the cutoff mass in the form factor, we employ $\Lambda = 800$ MeV. However, we performed test calculations where we varied the value of Λ by 10% in order to examine the sensitivity of our results to this phenomenological treatment. Fortunately, it turned out that the variations in the K^-d observables that we consider coming from the choice of the cutoff are negligibly small.

Partial-wave cross sections for $K^-n \to K^-n$ and $K^-p \to \bar{K}^0n$ of the KSU analysis [44] are displayed in Fig. 3. Obviously, for $p_{K^-} = 1$ GeV/c, i.e., the kinematics of the E31 experiment, there are large contributions from the $d_{I\,5}$ and $f_{I\,5}$ amplitudes, respectively. (We use here the standard notation $L_{I\,2J}$, but with small letters for the two-body amplitudes as it is commonly done in three-body calculations.)

For the deuteron wave function, ϕ_d, we use the one of the Nijmegen potential Nijm93 [45]. We tested wave functions from other realistic potentials too, but it turned out that the results are rather insensitive to the particular choice.

IV. RESULTS AND DISCUSSION

Before presenting the results, we briefly review our earlier studies on the $K^-d \to \pi\Sigma N$ reaction and relevant works. We started with a calculation of the two-step processes [31] for the beam momentum $p_K = 0.6$ GeV/c and the neutron angle $\theta_n = 0^\circ$, where the s waves of the Jülich meson-exchange model [15] and the ORB chiral interaction [10] were used for the $\bar{K}N - \pi\Sigma$ amplitude. The diagrams included in these calculations are depicted in Fig. 1. (The plane-wave impulse process, see Fig. 3(A) in Ref. [31], gives negligible effects and is not shown.) However, no clear peak was seen in the $\Lambda(1405)$ resonance region, and then we proceeded to a Faddeev calculation, which enabled us to sum up all rescattering processes. We performed calculations [29] for $p_{K^-} = 1$ GeV/c and $\theta_n = 0^\circ$ considering the kinematics of the J-PARC E31 experiment [27] and obtained converged results after the sixth

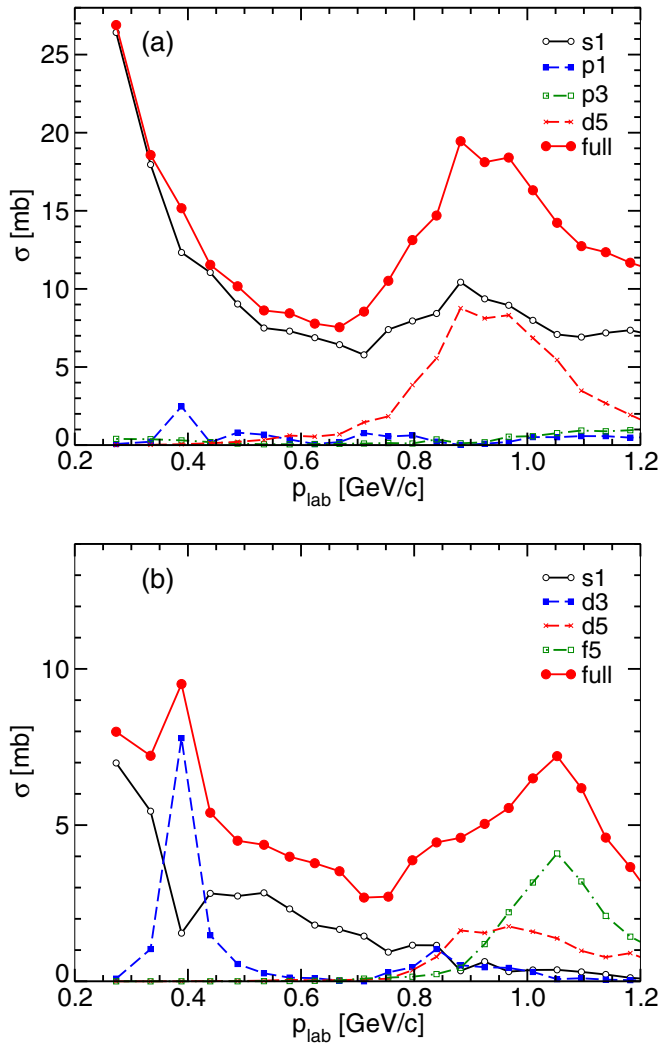

FIG. 3. Partial-wave cross sections of the KSU analysis [44] for (a) $K^-n \to K^-n$ and (b) $K^-p \to \bar{K}^0n$. The partial waves are indicated by L_{2J}.

iteration of Eqs. (11)–(13), where the same s-wave $\bar{K}N - \pi\Sigma$ interaction mentioned above was used. (The transition to the $\pi\Sigma N$ system was treated perturbatively.) Although a peak corresponding to the $\Lambda(1405)$ resonance appeared there, the line shape of the $\pi\Sigma$ invariant mass spectrum did not match the preliminary E31 results [25,26,46] and, in addition and more disturbingly, its magnitude was five times smaller than the experimental results.

Recently, Kamano and Lee [34] investigated the reaction $K^-d \to \pi\Sigma n$ as well and they realized the importance of the $\bar{K}N \to \bar{K}N$ amplitude that enters into the first rescattering process ($t^{\mathcal{I}}$ in Fig. 1). This amplitude is well constrained because there is a wealth of data in the high-energy region corresponding to the incoming K^- momentum of 1 GeV/c. Their calculation is based on the two-step processes depicted in Fig. 1 and they use amplitudes from their coupled-channel $\bar{K}N$ potential [17] which was developed in the course of a comprehensive analysis of $\bar{K}N$ data up to an energy of 2100 MeV. In their calculation, K^-d cross sections of comparable magnitude to the E31 experiment were obtained [34].

The results in Ref. [34] indicate very clearly that it is crucial to use the full amplitude for the initial $\bar{K}N \to \bar{K}N$ process, and not only the s-wave contribution as we [29,31] and others [30] did in the past. Thus, as already mentioned in Sec. III, in the present work we adopt the $\bar{K}N \to \bar{K}N$ amplitude established by the KSU group [44] which describes the $\bar{K}N$ reaction data in the high-energy region with similar or possibly even better quality than the one used in Ref. [34].

The merits of the special kinematics of the E31 experiment have been discussed thoroughly in Refs. [27,34]. In short, the K^- kicks out the neutron (or proton) from the deuteron and is thereby strongly slowed down. The slowly moving K^- interacts then with the remaining nucleon and converts into $\pi\Sigma$. Viewed in the c.m. frame, the outgoing nucleon and the $\pi\Sigma$ system move back to back [34], and therefore, there is basically no correlation between them. Another important aspect is that the energy regions in which the involved two subprocesses, $\bar{K}N \to \bar{K}N$ and $\bar{K}N \to \pi\Sigma$, take place are well separated for this special kinematics. Specifically, for $\pi\Sigma$ invariant masses below 1490 MeV, say, the region of interest where the majority of the E31 data are, the corresponding energy for $t^{\mathcal{I}}$, i.e., the $\bar{K}N \to \bar{K}N$ amplitude, is essentially above 1550 MeV or so, and thus well above the $\bar{K}N$ threshold. Therefore, there is no principle conflict when using the $\bar{K}N \to \bar{K}N$ amplitude from the partial-wave analysis and the $\bar{K}N \to \pi\Sigma$ amplitude from chirally motivated potentials. Finally, according to Kamano and Lee, only the s wave of the $\bar{K}N \to \pi\Sigma$ amplitude is of relevance for the considered observables, cf. Fig. 7 in Ref. [34]. Thus, it is meaningful to combine the full $\bar{K}N \to \bar{K}N$ amplitude from the KSU analysis and the s-wave $\bar{K}N \to \pi\Sigma$ amplitude from chiral potentials. Indeed, variations in the results reflect directly differences in the $\bar{K}N \to \pi\Sigma$ amplitude around and below the $\bar{K}N$ threshold as predicted by the chiral interactions. On the other hand, existing differences in the (s-wave) $\bar{K}N \to \bar{K}N$ amplitude in the near-threshold region [2] do not play a role for the actual results.

A. Comparison with preliminary E31 results

In Fig. 4, inclusive cross sections for the reaction $K^-d \to \pi\Sigma N$ are shown as a function of the $\pi\Sigma$ invariant mass. The K^- beam momentum and the neutron angle are fixed to $p_{K^-} = 1$ GeV and $\theta_n = 0^\circ$, respectively, in accordance with the J-PARC E31 experiment [25]. We use the amplitudes by the KSU group [44] for the $\bar{K}N \to \bar{K}N$ processes depicted as $t^{\mathcal{I}}$ in Fig. 1, while the chirally motivated interaction TW1 [35] by Cieplý and Smejkal is utilized for generating the $\bar{K}N \to \pi\Sigma$ amplitude that are represented by $t^{\mathcal{F}}$ in Fig. 1. Partial waves up to a total angular momentum of $j = 7/2$ are included for the $\bar{K}N \to \bar{K}N$ amplitude. Isospin-averaged masses are used so that the $\bar{K}N$ threshold is at 1434.6 MeV.

The predicted line shapes for the three final states in Fig. 4 are compared with available but still preliminary data of the E31 experiment [26]. In contrast to our former work [29], where only an s-wave interaction was used for the amplitude of the first step ($t^{\mathcal{I}}$), the cross sections increase drastically and reach a magnitude that is comparable to the experiment. The importance of using the full amplitude for $t^{\mathcal{I}}$ becomes

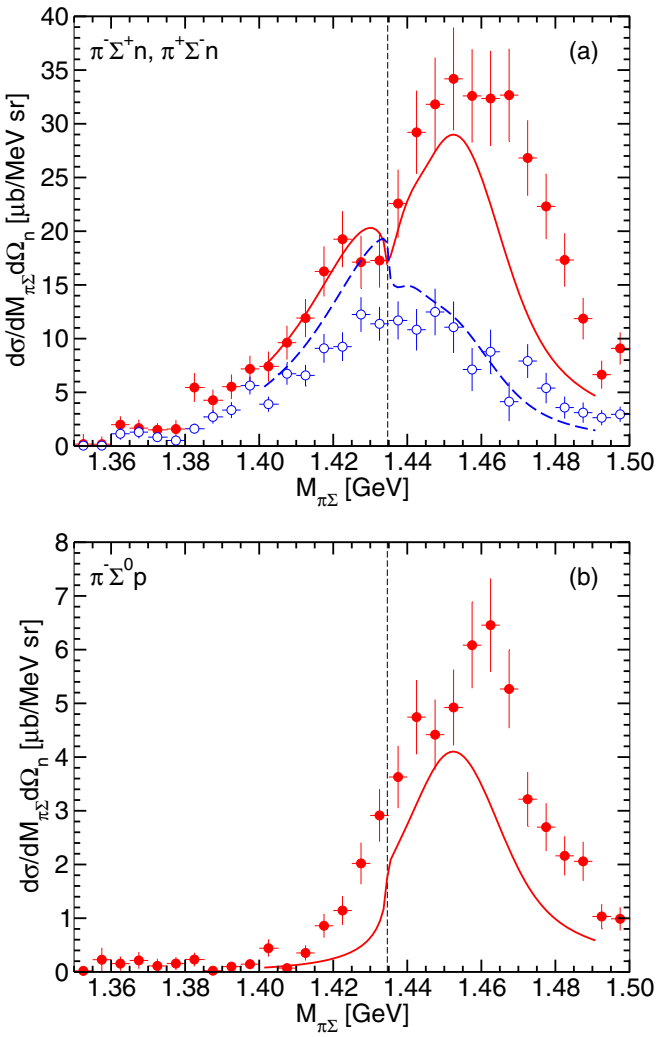

FIG. 4. Double differential cross section for (a) $\pi^{\pm}\Sigma^{\mp}n$ and (b) $\pi^-\Sigma^0 p$. Predictions based on the potential TW1 [35] are indicated by solid ($\pi^-\Sigma^+n$, $\pi^-\Sigma^0 p$) and dashed lines ($\pi^+\Sigma^-n$), respectively. Preliminary data are taken from Ref. [26]. Vertical line indicate the $\bar{K}N$ threshold.

immediately clear when one inspects the $\bar{K}N \to \bar{K}N$ cross section generating by the KSU amplitudes, displayed in Fig. 3. It can be seen that the partial waves $d_{I\,5}$ and $f_{I\,5}$ provide large contributions to the cross section around $p_K \approx 1$ GeV/c, the relevant energy region for the amplitude in the first step.

Indeed, in our new calculation there is a good overall agreement with the preliminary data for $K^-d \to \pi^-\Sigma^+n$. In particular, the maximum of the spectrum is roughly reproduced. Qualitatively, the results are similar to those reported by Kamano and Lee in Ref. [34].

B. Origin of the peaks: Quasifree scattering and Λ(1405)

Before analyzing the results in detail and examining also other potentials, let us discuss the origin of the structure of the line shape and, in particular, of the peaks. It can be understood by considering the amplitude for the two-step process, $t_{\pi\Sigma,\bar{K}N}\, G_0\, t_{\bar{K}N,\bar{K}N}\, \phi_d$ which is obtained after the iteration of the Faddeev equations (12) and (13). The structure results from an interplay between $t_{\pi\Sigma,\bar{K}N}$ and $G_0\, t_{\bar{K}N,\bar{K}N}\, \phi_d$. We present the moduli of those quantities in Fig. 5. The $\bar{K}N \to \pi\Sigma$ amplitude, shown here for different charge channels, exhibits a clear peak below the $\bar{K}N$ threshold which reflects the presence of the $\Lambda(1405)$ resonance. For $\pi\Sigma$ invariant masses above that threshold, it becomes smooth and rather small. Note that $K^-p \to \pi^0\Sigma^0$ (dashed line) corresponds to a pure ($I = 0$) isospin state. In the case of $K^-p \to \pi^+\Sigma^-$ and $K^-p \to \pi^-\Sigma^+$, there is an interference with the $I = 1$ state, with opposite signs, and accordingly the peak positions are shifted to somewhat higher or lower invariant masses. Moreover, the behavior at the $\bar{K}N$ threshold is different in the case of $K^-p \to \pi^-\Sigma^+$ (solid line); i.e., there is cusp and not a rounded step anymore. Together with the specific weighting by the term $G_0\, t_{\bar{K}N,\bar{K}N}\, \phi_d$, cf. Fig. 5(b), this causes the distinct differences in the cross sections for the $\pi^+\Sigma^-n$ and $\pi^-\Sigma^+n$ channels around the $\bar{K}N$ threshold.

The large peak of the $\pi^-\Sigma^+n$ cross section for energies around 1455 MeV is clearly coming from the combined effect of the Green's function and $t_{\bar{K}N,\bar{K}N}\, \phi_d$. It is due to quasifree scattering (QFS) of the K^- on the nucleons. The $\pi^+\Sigma^-n$ results are remarkably different, experimentally as well as in theory, reflecting large interferences between the $I = 0$ and $I = 1$ contributions. In the case of $K^-d \to \pi^-\Sigma^0 p$, a pure $I = 1$ state, QFS is likewise responsible for most of the structure, cf. Figs. 5(b) (dotted line) and 4(b). The $\bar{K}N \to \pi\Sigma$ amplitude with $I = 1$ corresponds to the dotted line in Fig. 5(a). There is a noticeable cusp at the $\bar{K}N$ threshold, and the drop of the amplitude below the threshold is partly responsible for the clear reduction of the $K^-d \to \pi^-\Sigma^0 p$ cross section in that energy region, but otherwise $t^{I=1}_{\pi\Sigma,\bar{K}N}$ exhibits a rather smooth behavior.

C. Sensitivity to differences between the chiral potentials

Given that the data from the E31 experiment are still preliminary, it is certainly too early for drawing more detailed conclusions. This should be kept in mind when we now compare the predictions based on different chiral potentials with each other and confront them also with those data. We consider here, besides the potential TW1, the interactions by Ohnishi *et al.* [30] and by Oset-Ramos-Bennhold [10]. Results are presented in Fig. 6.

As already discussed above, in our calculation based on TW1 the overall magnitude of the cross sections is well reproduced, for the $\pi^{\pm}\Sigma^{\mp}n$ channels as well as for $\pi^-\Sigma^0 p$. (Data for $\pi^0\Sigma^0 n$ have been already presented too [26], but are still very preliminary and no absolute values are given.) This is also the case for the two other potentials. At the same time, there are noticeable variations between the predictions for the different potentials. Since the same $\bar{K}N \to \bar{K}N$ amplitude is used in the calculations, these reflect differences in the pertinent $\bar{K}N \to \pi\Sigma$ amplitudes.

Let us first discuss the $\pi^-\Sigma^0 p$ spectrum which exhibits the simplest structure. In this channel, only the $I = 1$ component of $\pi\Sigma$ can contribute, and therefore one can trace back the features in the cross section directly to those of the two ingredients, $t^{I=1}_{\pi\Sigma,\bar{K}N}$ and $G_0\, t_{K^-p,K^-p}\, \phi_d$, shown in Figs. 2 and 5,

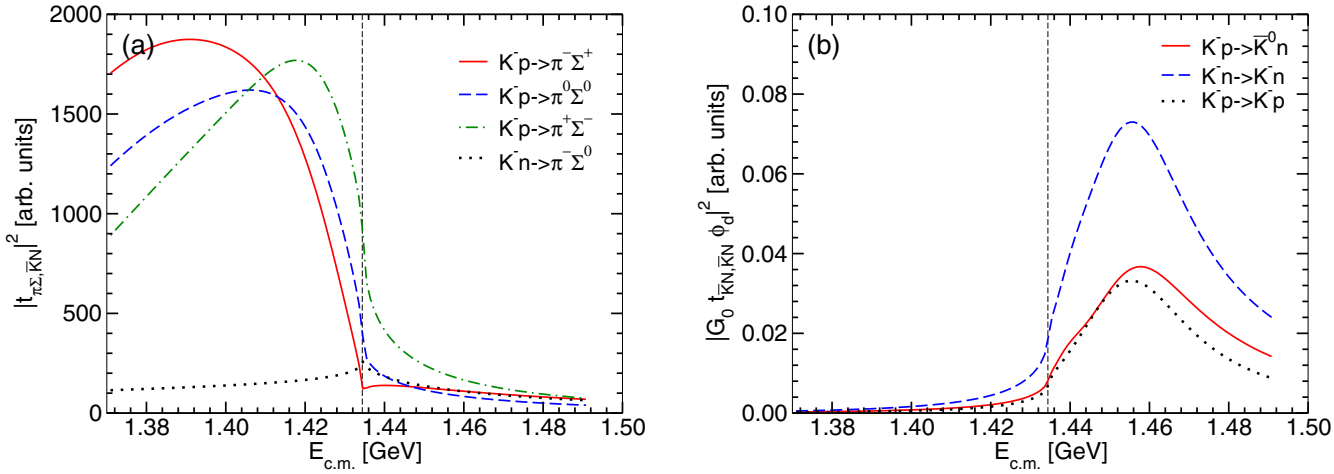

FIG. 5. The quantitities (a) $|t_{\pi\Sigma,\bar{K}N}|^2$ and (b) $|G_0\, t_{\bar{K}N,\bar{K}N}\, \phi_d|^2$ for different charge channels. The results shown are for the potential TW1 [35]. Vertical line indicate the $\bar{K}N$ threshold.

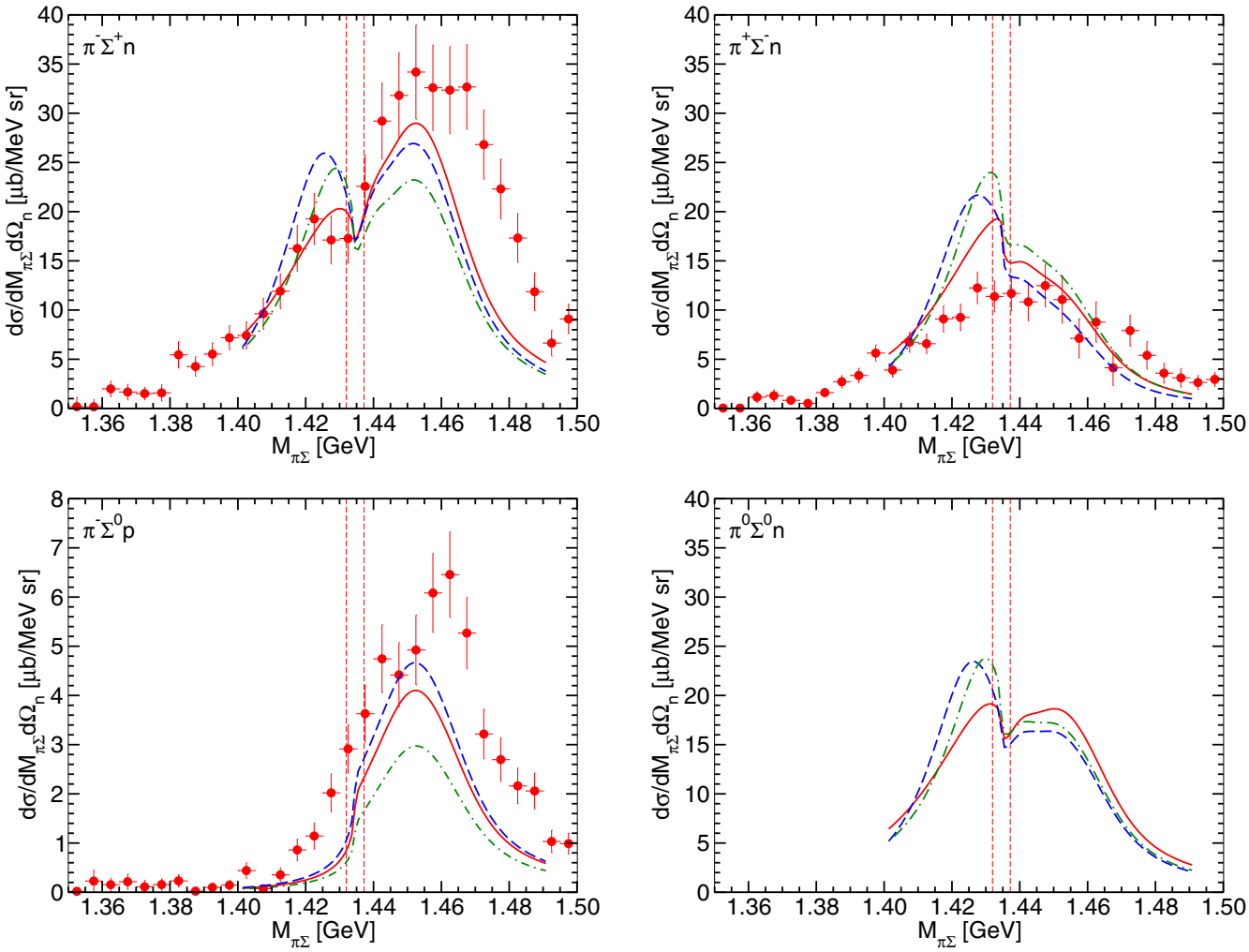

FIG. 6. Double differential cross section for $K^- d \to \pi\Sigma N$. Results are shown for the potentials of Cieplý and Smejkal [35] (solid lines), Ohnishi *et al.* [30] (dash-dotted lines), and Oset-Ramos-Bennhold [10] (dashed lines). Preliminary data are taken from Ref. [26]. Vertical lines indicate the $K^- p$ and $\bar{K}^0 n$ thresholds. Note that the scale for the $\pi^-\Sigma^0 p$ results is different.

respectively. Specifically, there is a one-to-one correspondence of the order of the maxima in the cross sections and the magnitudes of the $\bar{K}N \to \pi\Sigma$ amplitude in the relevant region of 1440–1460 MeV. The ORB potential provides the largest predictions for both.

The $\pi\Sigma$ invariant mass where the maximum occurs is basically determined by the product of the Green's function with $t_{\bar{K}N,\bar{K}N}\,\phi_d$ [cf. Fig. 5(b)] and, therefore, it is the same for all potentials. Indeed, also the maximum of the two model predictions in Ref. [34] is practically at the same invariant mass. It is somewhat surprising that the preliminary data suggest that the maximum could be at somewhat higher invariant masses. A shift of the maximum by 10–15 MeV would be rather difficult to achieve within our scheme. It would require a drastic change in the $\bar{K}N \to \bar{K}N$ or $\bar{K}N \to \pi\Sigma$ amplitudes. Certainly, one has to wait for the final analysis of the experiment in order to see whether this discrepancy will persist.

Interestingly, the $\pi^-\Sigma^0 p$ data do not show any effect from the opening of the $\bar{K}N$ channel. In the theoretical predictions there is a clear drop off in the cross section right below the $\bar{K}N$ threshold. As a consequence, there is a sizable underestimation of the preliminary data in that invariant-mass region.

The $\pi^-\Sigma^+ n$ and $\pi^+\Sigma^- n$ channels involve contributions from $I = 0$ and $I = 1$. The line shape for the former is quite well described by the predictions based on the potential TW1. This concerns not only the maximum but also the structure induced by the $\Lambda(1405)$ resonance. Specifically, the calculation produces a moderate peak at the corresponding invariant mass and a dip at the $\bar{K}N$ threshold, i.e. features that are reasonably well in line with the measurement. Only the peak position itself appears to be slightly closer to the $\bar{K}N$ threshold than what is indicated by the preliminary data. Obviously, the other two potentials generate a too pronounced structure so that the empirical information is drastically overestimated. Like for $\pi^-\Sigma^0 p$, there is also a noticeable underestimation of the empirical results for the $\pi^-\Sigma^+ n$ channel at higher invariant masses for all potentials. However, here the available empirical information points to a possible extended plateau rather than to an actual shift of the maximum as compared to the theoretical predictions.

In contrast to the channels discussed above, there is only a poor overall agreement with the preliminary data for $K^- d \to \pi^+\Sigma^- n$. Here the predictions are only roughly in line with the experiment for higher invariant masses. Around the $\bar{K}N$ threshold, the spectrum is significantly overestimated. Moreover, the structure produced in the three-body calculation does not resemble at all the behavior exhibited by the data. In the experiment, there is practically no effect seen from the opening of the $\bar{K}N$ channel, while theory produces a pronounced peak below the threshold for all considered potentials. Actually, the same incorrect behavior is present in the results by Kamano and Lee [34].

Finally, the results for $\pi^0\Sigma^0 n$ are qualitively similar to those for $\pi^-\Sigma^+ n$, except that there is a less pronounced maximum for invariant masses above the $\bar{K}N$ threshold. In this channel, only the $I = 0$ component of $\pi\Sigma$ can contribute, which makes it to the most promising one for exploring and pinning down the structure of the $\Lambda(1405)$ resonance.

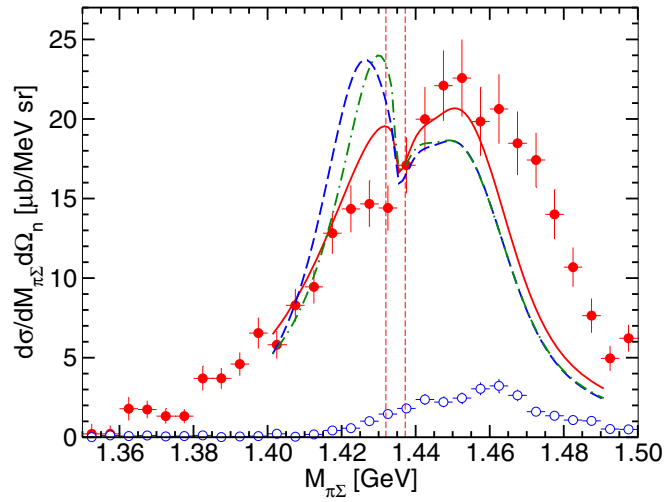

FIG. 7. Average of $K^- d \to \pi^+\Sigma^- n$ and $K^- d \to \pi^-\Sigma^+ n$ spectrum (lines, filled circles) vs half of the $K^- d \to \pi^-\Sigma^0 p$ spectrum (empty circles), cf. Eq. (26) and text. Same description of curves as in Fig. 6. Prelimary data are taken from Ref. [26]. Vertical lines indicate the $K^- p$ and $\bar{K}^0 n$ thresholds.

Following the experimentalists, we consider here in addition the average of the $K^- d \to \pi^+\Sigma^- n$ and $K^- d \to \pi^-\Sigma^+ n$ spectrum, cf. Fig. 7, denoted by $(\sigma_{\pi^+\Sigma^- n} + \sigma_{\pi^-\Sigma^+ n})/2$ to simplify the notation. Since [1]

$$\sigma_{\pi^\pm\Sigma^\mp n} \propto \frac{1}{3}|T_{I=0}|^2 + \frac{1}{2}|T_{I=1}|^2 \pm \frac{\sqrt{6}}{3}\mathrm{Re}\,(T_{I=0}T^*_{I=1}), \quad (26)$$

it is clear that in this average the interference term between the $I = 0$ and $I = 1$ contributions drops out. We want to emphasize, however, that the amplitudes T_I in Eq. (26) do not correspond directly to those for $\bar{K}N \to \pi\Sigma$, i.e., to $t^I_{\pi\Sigma,\bar{K}N}$. Formally, and ignoring the interdependence of the kinematical variables for which the amplitudes in the subsystems are evaluated, their relations are $T_{I=0} = t^{I=0}_{\pi\Sigma,\bar{K}N}/\sqrt{2} \times (A - B)$ and $T_{I=1} = t^{I=1}_{\pi\Sigma,\bar{K}N}/\sqrt{2} \times (A + B)$, where $A = G_0\, t_{K^0 n,K^- p}\phi_d$ and $B = G_0\, t_{K^- n,K^- n}\phi_d$. Here the relative signs reflecting whether the proton or neutron in the deuteron takes part in the scattering process have been already accounted for.

Furthermore, one should be aware that due to the large mass splitting between K^- and $\bar{K}^0$ [47], the physical thresholds of the $K^- p$ and $\bar{K}^0 n$ channels are separated by more than 5 MeV, as indicated in Fig. 7. Thus, there will be a potentially large breaking of the isospin symmetry in the region close to and between the $K^- p$ and $\bar{K}^0 n$ thresholds, making it impossible to define amplitudes with proper isospin. Consequently, caution is required when applying Eq. (26) for the interpretation of the data in that specific energy region.

Figure 7 includes also data for (half of) $\sigma_{\pi^-\Sigma^0 p}$ (empty circles). Since that cross section corresponds to $\frac{1}{2}|T_{I=1}|^2$, it is obvious that the $\pi^\pm\Sigma^\mp n$ results are dominated by the $I = 0$ component. Nevertheless, the individual results shown in Fig. 6 reveal that the $I = 1$ contribution is by no means negligible and plays a decisive role for the actual line shapes.

In view of the preliminary character of the data, it is premature to draw more concrete conclusions with regard to the properties of the elementary $\bar{K}N \to \pi\Sigma$ interaction. However, it is obvious that larger values of the $I = 1$ $\bar{K}N \to \pi\Sigma$ amplitude for invariant masses above the $\bar{K}N$ threshold would bring the maximum of the $\pi^-\Sigma^0 p$ cross section closer to the experiment and likely also the one for $\pi^-\Sigma^+ n$. Indeed, the KSU analysis supports larger values for the corresponding s-wave amplitude; see Fig. 2. Its absolute square exceeds the one predicted, e.g., by the ORB potential by about 30% at 1480 MeV.

The situation is more complicated below the $\bar{K}N$ threshold and, specifically, in the $\Lambda(1405)$ region. Still, the results shown in Figs. 6 and 7 provide a strong indication that the $\Lambda(1405)$ peaks by all three potentials are too large in magnitude. In particular, there is a dramatic overestimation in the sum of $\pi^+\Sigma^- n$ and $\pi^-\Sigma^+ n$, cf. Fig. 7, where interferences between the $I = 0$ and $I = 1$ amplitudes should cancel, at least to some extent and disregarding the potential difficulties with the isospin "interpretation" mentioned above.

D. Influence of three-step processes

In the course of our calculation, we explored also contributions from three-step processes, where the corresponding amplitudes are obtained by iterating twice the Faddeev equations (11)–(15). As already mentioned, we needed several iterations to reach converged results in case when only the s-wave $\bar{K}N \to \bar{K}N$ amplitude was included [29]. In contrast, now where $\bar{K}N$ partial waves up to $j = 7/2$ are incorporated, there are practically no visible changes in the invariant-mass spectra at 0° of the outgoing neutron when the three-step processes are included. Let us provide exemplary results for the two processes shown in Fig. 8 which are expected to yield the largest effects among the three-step processes. We use the Nijmegen potential Nijm93 [45] for the NN sector, and include partial waves up to $j = 3$. It turned out that the process in Fig. 8(b) gives larger contributions than the process

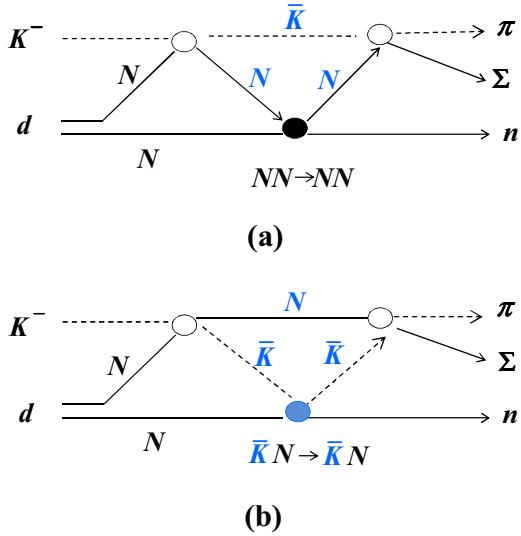

FIG. 8. Diagrams for three-step processes

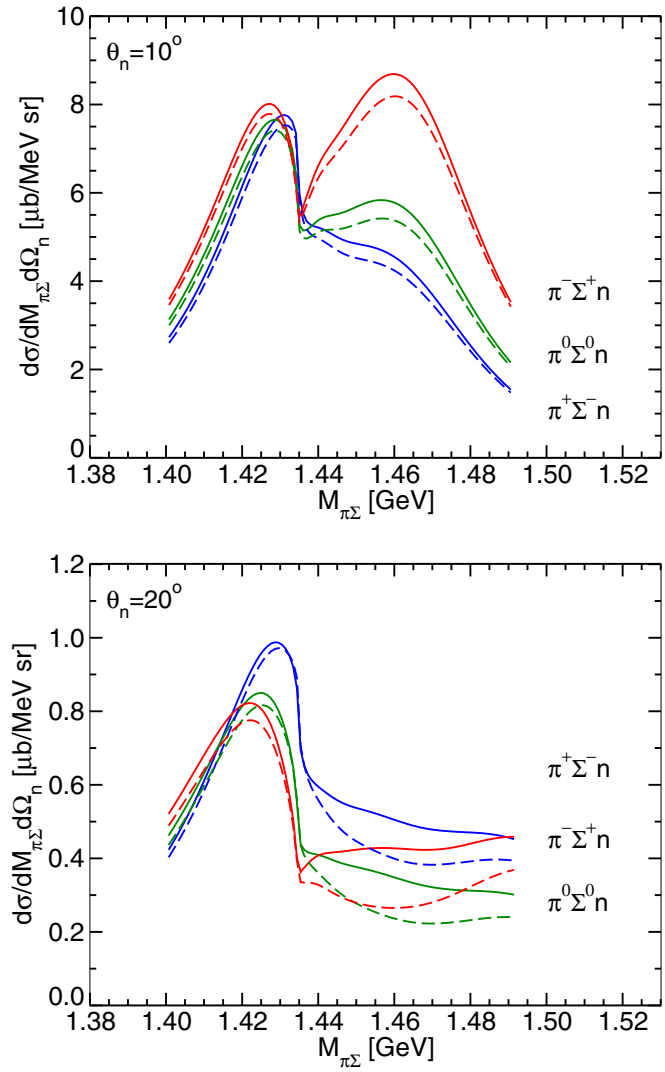

FIG. 9. $K^-d \to \pi\Sigma n$ results for neutron angles $\theta_n = 10°$ and 20°. Results based on two-step processes only (solid lines) are shown together with those where three-step processes are also included (dashed lines). The predictions are based on the potential TW1 [35].

in Fig. 8(a) with the NN interaction, but still the overall effect is tiny for $\theta_n = 0°$ and the spectra remain almost unchanged as compared to the results for the two-step processes. Therefore, we extended the calculations to $\theta_n = 10°$ and 20° for further exploration. Corresponding results including the process in Fig. 8(b) are shown in Fig. 9. With increasing neutron angle, the peak originating from $\bar{K}N$ QFS is more reduced and the structure due to the $\Lambda(1405)$ becomes more pronounced. However, at the same time, the overall magnitude of the cross section is strongly reduced, which makes corresponding experiments much more challenging.

V. SUMMARY

In this paper, we reported on a calculation of the reaction $K^-d \to \pi\Sigma N$ within a Faddeev-type approach. The work is motivated by corresponding experiments that are presently performed at J-PARC. Accordingly, spectra for various charge

channels of the $\pi\Sigma$ final state were presented for the specific kinematics of the E31 experiment [27], namely for the K^- beam momentum of $p_K = 1$ GeV/c and the neutron angle of $\theta_n = 0^\circ$. A comparison with preliminary data that have become available recently [25,26] was performed.

The employed Faddeev-type approach requires as main input amplitudes for the two-body subsystems $\bar{K}N \to \bar{K}N$ and $\bar{K}N \to \pi\Sigma$. For the latter, we utilized results generated from so-called chiral unitary models taken from the literature. Specifically, we used the potentials by Cieplý and Smejkal (TW1) [35] and Ohnishi *et al.* ($V^{E-\text{dep.}}$) [30], both of which are constrained by the latest measurement of kaonic hydrogen [8], and a more historical potential that is due to Oset *et al.* [10]. On the other hand, the $\bar{K}N \to \bar{K}N$ amplitude was taken from a recent partial-wave analysis [44] because of the following reason: While in the calculation of the quantities measured in the E31 experiment the $\bar{K}N \to \pi\Sigma$ amplitude is sampled at energies around the $\bar{K}N$ threshold, the $\bar{K}N \to \bar{K}N$ amplitude is probed in an entirely different kinematical regime. It is required for c.m. energies corresponding to the initial momentum of $p_K = 1$ GeV/c, which means around 1800 MeV. The aforementioned chiral potentials do not provide a realistic description of $\bar{K}N$ scattering at such high energies. Moreover, in that energy region higher partial waves yield an essential contribution, not only for $\bar{K}N$ elastic scattering but also in the reaction $K^-d \to \pi\Sigma N$ that is investigated here. The latter aspect has become clear after the pioneering work of Kamano and Lee [34], and it has been confirmed in the present study. Chiral potentials are typically limited to s waves. Thus, calculations that employ such models for the $\bar{K}N \to \pi\Sigma$ as well as the $\bar{K}N \to \bar{K}N$ amplitudes—like ours [31] and several others in the past—allow only very limited access to the physics that governs the E31 experiment.

The predictions of our calculations turned out to agree quite well with the preliminary data on a qualitative level, i.e., as far as the magnitude and the line shape in general is concerned. Especially, the spectra for $K^-d \to \pi^-\Sigma^+n$ and $K^-d \to \pi^-\Sigma^0p$ are fairly close to the data reported so far. However, on a more quantitative level, there are noticeable differences. In particular, the situation with regard to the structure of the $\Lambda(1405)$—the prime motivation behind the E31 experiment—is conflicting. Indeed, all three potentials produce a structure in the relevant $\pi\Sigma$ invariant-mass region; however, it is much too pronounced as compared to what is indicated presently by the measurement. Actually, in case of $\pi^+\Sigma^-n$ even the line shape is quite different.

Given the preliminary status of the data, it is obvious that the present study can only have an exploratory character and that solid conclusions, specifically with regard to the structure of the $\Lambda(1405)$ resonance, have to be postponed. Nonetheless, it has become clear that the general conditions are similar to what has been already found in studies of other reactions with the aim of scrutinizing the structure of the $\Lambda(1405)$ [48–50], namely that the line shape around the $\bar{K}N$ threshold is a result of (a) a delicate interplay between the isospin $I = 0$ and $I = 1$ $\bar{K}N \to \pi\Sigma$ amplitudes, and (b) the energy dependence of the subthreshold $I = 0$ $\bar{K}N$ amplitude or, equivalently, the pole structure of the $\Lambda(1405)$. Disentangling these two aspects remains a challenge. In any case, the observed differences between the employed potentials are promising for the prospect of getting further constraints on the $\bar{K}N$ interaction in the $\Lambda(1405)$ resonance region and, specifically, on the $\bar{K}N \to \pi\Sigma$ transition amplitude. Of course, whether final conclusions on the $\Lambda(1405)$ will be possible depends not least on the accuracy of the data that is eventually achieved in the E31 experiment. The most promising channel would be $K^-d \to \pi^0\Sigma^0n$, where the emerging $\pi^0\Sigma^0$ system is in a pure isospin $I = 0$ state. However, with only neutral particles in the final state it is obviously also by far the most ambitious one for an experiment [26].

ACKNOWLEDGMENTS

We acknowledge communication with A. Cieplý and M. Mai with regard to their $\bar{K}N$ interactions.

APPENDIX A: PERMUTATION OPERATOR

We use the Balian-Brézin [40,51] approach to calculate the permutation matrix element in Eq. (21). Since the details of the derivation for the nonrelativistic case are given in Ref. [39], we concentrate on an extension to the relativistic case and only show its final expression. In Sec. II B, $\langle k'q\,\alpha'|P_{23}|\,k''q''\alpha''\rangle$ appears, but a cyclic permutation $P_{23}P_{13}$ often used is considered because $\langle k'q\,\alpha'|\,P_{23}$ is easily obtained from $\langle k'q\,\alpha'|\,P_{23}P_{13}$ by a permutation inside the two-body sector.

First, we introduce the momentum state of the noninteracting particles 1 and 2 in the two-body c.m. frame which is associated with individual momenta via

$$|\vec{k}'';\vec{0}\rangle \equiv |\vec{k}''\rangle\,|-\vec{k}''\rangle.$$

On the left-hand side, the relative momentum $\vec{k}''$ and the total momentum zero are indicated. This is boosted to the three-body c.m. frame and expressed together with the third particle (numbered 3) state $|\vec{q}\,''\rangle$ as

$$|\vec{k}'';-\vec{q}\,''\rangle\,|\vec{q}\,''\rangle\,,$$

where the Wigner rotations for spins are neglected. The permutation matrix element between these states can be evaluated by using Eq. (19) as

$$\begin{aligned}&\langle\vec{k}';-\vec{q}\,|\,\langle\vec{q}\,|\;P_{23}P_{13}\;|\vec{k}'';-\vec{q}\,''\rangle\,|\vec{q}\,''\rangle\\&=\delta(\vec{k}'-\rho\,\vec{q}-\vec{q}\,'')\,\delta(\vec{k}''+\vec{q}+\rho''\vec{q}\,'')\,\delta(\vec{q}+\vec{q}\,''+\vec{q}_1)\\&\quad\times N^{-\frac{1}{2}}N''^{-\frac{1}{2}},\end{aligned}\tag{A1}$$

where

$$N=\left|\frac{\partial(\vec{q''},\vec{q}_1)}{\partial(-\vec{q},\vec{k}')}\right|=\frac{W_{31}}{\omega_{31}}\,\frac{\omega_3(q'')\,\omega_1(q_1)}{u_3(k')\,u_1(k')}$$

is the Jacobian [52] for the Lorentz transformation from $(\vec{q}\,'',\vec{q}_1)$ to $(-\vec{q},\vec{k}')$. Similarlily,

$$N''=\left|\frac{\partial(\vec{q}_1,\vec{q})}{\partial(-\vec{q}\,'',\vec{k}'')}\right|=\frac{W_{12}}{\omega_{12}}\,\frac{\omega_1(q_1)\,\omega_2(q)}{u_1(k'')\,u_2(k'')},$$

where $\omega_i(q)=\sqrt{q^2+m_i^2}$, $u_i(k')=\sqrt{k'^2+m_i^2}$, $W_{31}=u_3(k')+u_1(k')$, $W_{12}=u_1(k'')+u_2(k'')$, and $\omega_{ij}=\omega_i+\omega_j$ for $i,j=1,2,3$.

Equation (A1) is of similar form as the one defined with Jacobi momenta in the nonrelativistic case, except for the

Jacobians, but ρ and ρ'' are no longer constants. Those are expressed as

$$\rho = \frac{1}{W_{31}}\left\{\frac{-\vec{k}'\cdot\vec{q}}{\omega_{31}+W_{31}} + u_3(k')\right\} \tag{A2}$$

and

$$\rho'' = \frac{1}{W_{12}}\left\{\frac{\vec{q}\cdot\vec{q}\,''}{\omega_{12}+W_{12}} + \omega_2(q)\right\}. \tag{A3}$$

We do not want to go into further details in this paper, but we mention that the Jacobians N, N'' and ρ, ρ'' are expressed by only three variables k', q, and x, where x is defined as $x \equiv \hat{k}'\cdot\hat{q}$.

On the basis of the above results, the permutation matrix element between partial-wave projected basis states $\langle k'q\,\alpha|P_{23}P_{13}|k''q''\alpha'\rangle$ can be evaluated in line with Appendix A in [39]. The resulting form is

$$\langle k'q\,\alpha\,|\,P_{23}P_{13}|\,k''q''\alpha'\rangle = \int_{-1}^{1} dx\,\frac{\delta(q''-\chi)}{q''^2}\,\frac{\delta(k''-\pi)}{k''^2}\,\bar{R}_{\alpha\alpha'}(k'q\,x), \tag{A4}$$

where χ and π are given in Eqs. (22), (23), and

$$\bar{R}_{\alpha\alpha'}(k'q\,x) = N^{-\frac{1}{2}}N''^{-\frac{1}{2}}\sqrt{\hat{j}\,\hat{j}_s\,\hat{j}'\,\hat{j}'_s}\sum_{LS}\hat{S}\begin{Bmatrix} l & s & j \\ \lambda & s_2 & j_s \\ L & S & J\end{Bmatrix}\begin{Bmatrix} l' & s' & j' \\ \lambda' & s_3 & j'_s \\ L & S & J\end{Bmatrix}(-)^{s_2+2s_3+s'}\sqrt{\hat{s}\hat{s}'}\begin{Bmatrix} s_3 & 0 & s \\ s_2 & S & s'\end{Bmatrix}$$

$$\times 8\pi^2\sum_{m_l\,m_{l'}\,m_{\lambda'}}(l\,\lambda\,L, m_l\,0\,m_l)\,(l'\,\lambda'\,L, m_{l'}\,m_{\lambda'}\,m_l)(-)^{m_l}Y_{l\,-m_l}(\hat{k}')Y_{l'\,m_{l'}}(\hat{k}'')Y_{\lambda'\,m_{\lambda'}}(\hat{q}'')\sqrt{\frac{2l+1}{4\pi}}. \tag{A5}$$

We use the notation $\hat{j} \equiv 2j+1$ and assume that $\vec{q}$ is along the z axis and $\vec{k}'$ lies in the x-z plane. The two vectors $\vec{k}''$ and $\vec{q}\,''$ are defined as

$$\vec{q}\,'' = \vec{k}' - \rho\,\vec{q},$$
$$\vec{k}'' = -\rho''\vec{k}' - (1-\rho''\rho)\,\vec{q}.$$

Finally, $R_{\alpha\alpha'}$ in Eq. (21) is related to $\bar{R}_{\alpha\alpha'}$ by

$$R_{\alpha\alpha'}(k'q\,x) = (-)^l\bar{R}_{\alpha\alpha'}(k'q\,x),$$

where the phase is easily obtained by applying P_{13} on $\langle k'q\,\alpha|\,P_{23}$ to the left as mentioned above.

APPENDIX B: ANALYTICAL INTEGRATION OVER x AND k'' AND THE DOMAIN FOR THE k' AND q'' INTEGRATIONS

Here we describe how the x and k'' integrations are performed analytically in Eq. (20) and how the domain for the k' and q'' integrations is defined in Eq. (24). The major advantage of choosing x and k'' variables for analytic integrations is that it enables us to avoid moving singularities, which are well known to be difficult to treat in three-body calculations. This prescription was presented in Sec. 2.2 of Ref. [39] for the nonrelativistic case which is somewhat simpler. We explain how to extend it to the relativistic case and show only the formulas without going into details with regard to the numerical calculations.

In order to rewrite $\delta(q''-\chi)$ in Eq. (21) in the form where x is explicitly shown, first we deform ρ given in Eq. (A2) as follows:

$$\rho = \sigma(1-\delta x), \tag{B1}$$

where

$$\sigma = \frac{u_3(k')}{W_{31}}, \quad \delta = \frac{k'q}{u_3(k')(\omega_{31}+W_{31})}.$$

Notice that σ and δ are functions of k' and q. Then $\delta(q''-\chi)$ is rewritten as

$$\delta(q''-\chi) = \frac{q''}{k'\rho\,q f_r}\,\delta(x-x_0)\,\Theta(1-|x_0|), \tag{B2}$$

where

$$f_r = \left|1+\frac{\sigma q}{k'}\,\delta - \frac{\delta\,x_0}{1-\delta\,x_0}\right|$$

and x_0 is a solution of

$$q''^2 = k'^2 + \rho^2q^2 - 2k'\rho\,qx \tag{B3}$$

[see Eq. (22)]. Since ρ is a linear function of x, Eq. (B3) has actually two solutions, but one of them turns out to be physically meaningless. We omit the lengthy expression of x_0 here, but mention that it is a function of k', q and q''.

Using the two δ functions, $\delta(x-x_0)$ and $\delta(k''-\pi)$ we can perform the x and k'' integration analytically in Eq. (20). Note that the Θ function in Eq. (B2) restricts and defines the domain for the double integrations over k' and q''. In the nonrelativistic case, ρ is a constant [$\rho = m_3/(m_3+m_1)$] and the domain is easily deduced from Eq. (B3) and $|x_0| \leqslant 1$. It becomes an open rectangular region in the k'-q'' plane restricted by the three straight lines, $q'' = k' - \rho\,q$ and $q'' = \pm k' + \rho\,q$ (see Fig. 1 in Ref. [39]). In the relativistic case, ρ [$=\sigma(1-\delta x_0)$] depends on k', q, and x_0, namely k', q, and q'', and the boundaries of the "rectangle" are no longer straight lines but curves. Those are given by

$$q'' = \;\; k' + \rho_-\,q,$$
$$q'' = \;\; k' - \rho_+\,q,$$
$$q'' = -k' + \rho_+\,q.$$

where $\rho_- = \sigma(1+\delta)$ and $\rho_+ = \sigma(1-\delta)$. Thus we arrive at the expressions in Eq. (24).

[1] T. Hyodo and D. Jido, Prog. Part. Nucl. Phys. **67**, 55 (2012).
[2] A. Cieplý, M. Mai, U.-G. Meißner, and J. Smejkal, Nucl. Phys. A **954**, 17 (2016).
[3] Y. Kamiya, K. Miyahara, S. Ohnishi, Y. Ikeda, T. Hyodo, E. Oset, and W. Weise, Nucl. Phys. A **954**, 41 (2016).
[4] Y. Sada *et al.* (J-PARC E15 Collaboration), Prog. Theor. Exp. Phys. **2016**, 051D01 (2016).
[5] T. Sekihara, E. Oset, and A. Ramos, Prog. Theor. Exp. Phys. **2016**, 123D03 (2016).
[6] A. Gal, E. V. Hungerford, and D. J. Millener, Rev. Mod. Phys. **88**, 035004 (2016).
[7] N. V. Shevchenko, Few-Body Syst. **58**, 6 (2017).
[8] M. Bazzi *et al.* (SIDDHARTA Collaboration), Phys. Lett. B **704**, 113 (2011).
[9] J. A. Oller and U.-G. Meißner, Phys. Lett. B **500**, 263 (2001).
[10] E. Oset, A. Ramos, and C. Bennhold, Phys. Lett. B **527**, 99 (2002); **530**, 260(E) (2002).
[11] Y. Ikeda, T. Hyodo, and W. Weise, Nucl. Phys. A **881**, 98 (2012).
[12] Z.-H. Guo and J. A. Oller, Phys. Rev. C **87**, 035202 (2013).
[13] M. Mai and U.-G. Meißner, Nucl. Phys. A **900**, 51 (2013).
[14] S. Ohnishi, Y. Ikeda, H. Kamano, and T. Sato, Phys. Rev. C **88**, 025204 (2013).
[15] A. Müller-Groeling, K. Holinde, and J. Speth, Nucl. Phys. A **513**, 557 (1990).
[16] J. Haidenbauer, G. Krein, U.-G. Meißner, and L. Tolos, Eur. Phys. J. A **47**, 18 (2011).
[17] H. Kamano, S. X. Nakamura, T.-S. H. Lee, and T. Sato, Phys. Rev. C **90**, 065204 (2014).
[18] J. Zmeskal *et al.*, Acta Phys. Pol. B **46**, 101 (2015).
[19] K. Moriya *et al.* (CLAS Collaboration), Phys. Rev. C **87**, 035206 (2013).
[20] K. Moriya *et al.* (CLAS Collaboration), Phys. Rev. C **88**, 045201 (2013).
[21] H. Y. Lu *et al.* (CLAS Collaboration), Phys. Rev. C **88**, 045202 (2013).
[22] I. Zychor *et al.*, Phys. Lett. B **660**, 167 (2008).
[23] G. Agakishiev *et al.* (HADES Collaboration), Phys. Rev. C **87**, 025201 (2013).
[24] S. Prakhov, B. M. K. Nefkens, C. E. Allgower, V. Bekrenev, W. J. Briscoe, M. Clajus, J. R. Comfort, K. Craig, D. Grosnick, D. Isenhower *et al.*, Phys. Rev. C **70**, 034605 (2004).
[25] S. Kawasaki *et al.*, JPS Conf. Proc. **13**, 020018 (2017).
[26] K. Inoue *et al.*, presentation at the International workshop on Hadron and Nuclear Physics, Osaka, Japan, 12–14 March 2017 [https://indico2.riken.jp/indico/contributionDisplay.py?contribId=43&confId=2389]
[27] S. Ajimura *et al.* [http://j-parc.jp/researcher/Hadron/en/pac_1207/pdf/E31_2012-9.pdf]
[28] J. Revai, Phys. At. Nucl. **77**, 509 (2014).
[29] K. Miyagawa and J. Haidenbauer, JPS Conf. Proc. **17**, 072005 (2017).
[30] S. Ohnishi, Y. Ikeda, T. Hyodo, and W. Weise, Phys. Rev. C **93**, 025207 (2016).
[31] K. Miyagawa and J. Haidenbauer, Phys. Rev. C **85**, 065201 (2012).
[32] J. Yamagata-Sekihara, T. Sekihara, and D. Jido, Prog. Theor. Exp. Phys. **2013**, 043D02 (2013).
[33] D. Jido, E. Oset, and T. Sekihara, Eur. Phys. J. A **49**, 95 (2013).
[34] H. Kamano and T.-S. H. Lee, Phys. Rev. C **94**, 065205 (2016).
[35] A. Cieplý and J. Smejkal, Nucl. Phys. A **881**, 115 (2012).
[36] W. Glöckle and K. Miyagawa, Few-Body Syst. **30**, 241 (2001).
[37] W. Glöckle, H. Witala, D. Hüber, H. Kamada, and J. Golak, Phys. Rep. **274**, 107 (1996).
[38] R. Fong and J. Sucher, J. Math. Phys. **5**, 456 (1964).
[39] H. Witala and W. Glöckle, Eur. Phys. J. A **37**, 87 (2008).
[40] B. D. Keister and W. N. Polyzou, Phys. Rev. C **73**, 014005 (2006).
[41] H. Kamada, W. N. Polyzou, H. Witala, and K. Miyagawa, Few-Body Syst. **55**, 1079 (2014).
[42] N. Kaiser, P. B. Siegel, and W. Weise, Nucl. Phys. A **594**, 325 (1995).
[43] A. Cieplý and J. Smejkal, Eur. Phys. J. A **43**, 191 (2010).
[44] H. Zhang, J. Tulpan, M. Shrestha, and D. M. Manley, Phys. Rev. C **88**, 035204 (2013).
[45] V. G. J. Stoks, R. A. M. Klomp, C. P. F. Terheggen, and J. J. de Swart, Phys. Rev. C **49**, 2950 (1994).
[46] K. Inoue *et al.*, JPS Conf. Proc. **17**, 072003 (2017).
[47] Particle Data Group, C. Patrignani *et al.*, Chin. Phys. C **40**, 100001 (2016).
[48] L. Roca and E. Oset, Phys. Rev. C **88**, 055206 (2013).
[49] S. X. Nakamura and D. Jido, Prog. Theor. Exp. Phys. **2014**, 023D01 (2014).
[50] M. Mai and U.-G. Meißner, Eur. Phys. J. A **51**, 30 (2015).
[51] R. Balian and E. Brézin, Nuovo Cimento B **61**, 403 (1969).
[52] H. Witala, J. Golak, W. Glöckle, and H. Kamada, Phys. Rev. C **71**, 054001 (2005).